ELSEVIER

Microporous and Mesoporous Materials 44–45 (2001) 697–707

MICROPOROUS AND MESOPOROUS MATERIALS

www.elsevier.nl/locate/micromeso

Capillary condensation in MMS and pore structure characterization

Alexander V. Neimark *, Peter I. Ravikovitch

TRI/Princeton, 601 Prospect Avenue, P.O. Box 625, Princeton NJ 08542-0625, USA

Received 19 April 2000; accepted 25 August 2000

Abstract

Phenomena of capillary condensation and desorption in siliceous mesoporous molecular sieves (MMS) with cylindrical channels are studied by means of the non-local density functional theory (NLDFT). The results are compared with macroscopic thermodynamic approaches based on Kelvin–Cohan (KC) and Derjaguin–Broekhoff–de Boer (DBdB) equations. We show that: The KC equations, which constitute the basis of the traditional BJH method for the pore size distribution analysis, are in error even in pores as large as 20 nm. The DBdB equations with consistently determined thickness of the adsorbed layer (disjoining pressure isotherm) can be justified for pores wider than $\approx$7 nm in diameter. As the pore size decreases, the macroscopic arguments become less accurate, and the NLDFT and DBdB results differ significantly in pores smaller than $\approx$4 nm. The adsorption–desorption isotherms predicted by NLDFT are found to be in quantitative agreement with the experimental nitrogen (77 K) and argon (87 K) isotherms on MCM-41 type materials with pores larger than 5 nm. Therewith, the experimental desorption branch corresponds to the equilibrium capillary condensation/evaporation transition. The experimental adsorption branch corresponds to the spontaneous spinodal condensation, which occurs at the limit of stability of adsorption films. The NLDFT method has been developed for the calculation of pore size distributions from both the adsorption and desorption isotherms.

Keywords: Nitrogen adsorption; Argon adsorption; Capillary condensation; Density functional theory; Disjoining pressure; Hysteresis; Mesopores; MCM-41; Pore size distribution

1. Introduction

The capillary condensation of vapors is the primary method of assessment of structural parameters of mesoporous molecular sieves (MMS) and other materials with pores in the range of 2–100 nm [1,2]. Capillary condensation is associated with a shift in the vapor–liquid coexistence in pores compared to the bulk fluid [3,4] (for a recent review see e.g. Ref. [5]). A fluid confined in a pore condenses at a pressure lower than the saturation pressure at a given temperature. The condensation pressure depends on the pore size and shape and also on the strength of the interaction between the fluid and pore walls. It is assumed that for the pores of a given shape and surface chemistry, there exists a one-to-one correspondence between the condensation pressure and the pore diameter. Thus, the adsorption isotherm that represents the amount of

* Corresponding author. Tel.: +1-609-430-4818; fax: +1-609-683-7149.

E-mail address: aneimark@triprinceton.org (A.V. Neimark).

1387-1811/01/$ - see front matter
PII: S1387-1811(01)00251-7

adsorbed fluid as a function of the vapor pressure contains direct information about the pore size distribution in the sample. The idea of using the capillary condensation phenomenon for assessing the porosity of solids dates back to Zsigmondy [6], and at present, commercial automated adsorption instruments are equipped with the software for producing pore size distributions. However, despite its long history, the issue of reliable interpretation of adsorption isotherms remains still topical and attracts a great deal of attention from both experimentalists and theoreticians. This is one example where the solution of practical problems emerging in modern nanotechnology requires the solution of fundamental theoretical problems of fluid behavior in confining geometries.

Two interrelated problems are of fundamental interest. First, as well-documented in recent experiments with ordered MCM-41 materials, the classical theories of capillary condensation based on the Kelvin equation and its modifications [7,8] fail when applied to the nanoscale [9,10]. Secondly, in the vast majority of cases, capillary condensation occurs irreversibly, exhibiting hysteretic behavior [11], and, thus, causes an ambiguity in pore size characterization. The distribution functions calculated from the adsorption and desorption branches of the isotherm differ significantly. In recent years, many efforts have been devoted to the development of a quantitative theory of capillary condensation in nanopores using methods of statistical mechanics, which include Monte Carlo (MC) simulations [5,12–15], molecular dynamics [16,17], and density functional theory (DFT) [5,9,15,18–23]. At the same time, there have been many attempts to modify thermodynamic methods [24–28] which are based on macroscopic theories of capillary condensation in cylindrical pores formulated in the seminal works of Derjaguin [29,30], Broekhoff and de Boer [31–34], and Saam and Cole [35].

In this paper, we employ the non-local density functional theory (NLDFT) for modeling nitrogen (77 K) and argon (87 K) adsorption in cylindrical pores of siliceous MMS. The capillary condensation and evaporation pressures predicted by NLDFT are compared with the results of the Derjaguin–Broekhoff–de Boer (DBdB) theory to determine the range of validity of the macroscopic approach. It is demonstrated that the microscopic and macroscopic methods are in agreement for pores wider than $\approx$7 nm and deviate significantly for pores narrower than 4–5 nm. We also compare the NLDFT isotherms with the experimental adsorption–desorption isotherms on the MMS of MCM-41 type. In our previous publications [9,20], it was shown that the NLDFT model quantitatively describes equilibrium condensation/evaporation of nitrogen (77 K) and argon (77 and 87 K) isotherms on reference MCM-41 samples with cylindrical pore channels of 2–4.5 nm in width. Later, we found quantitative agreement for both adsorption and desorption branches of the isotherms in pores wider than $\approx$5 nm [15,22,23] using as examples nitrogen adsorption at 77.4 K on enlarged MCM-41 type materials [36–38]. Recently, Ar adsorption–desorption data at 87.3 K on some of these samples were published [39]. It was tempting to check the consistency of the NLDFT model by comparing the calculated and experimental Ar adsorption–desorption isotherms. The results presented below show that the Ar hysteresis loops can be quantitatively described using the same pore structure parameters which were previously employed for modeling N_2 adsorption.

2. Macroscopic theories of capillary condensation hysteresis in cylindrical pores

2.1. Kelvin–Cohan (KC) equations

According to Cohan [7], the capillary condensation in an infinite cylindrical pore is described by the Kelvin equation for the cylindrical interface between the adsorbed film and vapor,

$$RT\ln(P_A/P_0) = -\frac{\gamma V_L}{R_P - h_A} \tag{1}$$

while evaporation/desorption is associated with the formation of a hemispherical meniscus between the condensed fluid and vapor,

$$RT\ln(P_D/P_0) = -\frac{2\gamma V_L}{R_P - h_D} \tag{2}$$

Here P_A/P_0 and P_D/P_0 are the relative pressures of adsorption and desorption, respectively; γ and V_L

are the surface tension and the molar volume of the bulk liquid; R_P is the pore radius; h_A and h_D are the adsorption film thicknesses at the relative pressures P_A/P_0 and P_D/P_0 respectively. When the difference between the film thicknesses h_A and h_D is small compared to the pore radius, the width of the hysteresis is given by

$$P_D/P_0 = (P_A/P_0)^2 \tag{3}$$

The KC equation (2) constitutes the basis of the conventional BJH method for pore size calculations [8]. In so doing, the film thickness is considered as a given function of the relative pressure. This function, $h(P/P_0)$, represents the adsorption isotherm per unit area of the non-porous surface.

2.2. Derjaguin–Broekhoff–de Boer theory

The DBdB theory leads to capillary condensation and desorption pressures, which differ substantially from those of Cohan's equations, even in relatively large pores. The DBdB theory takes into account the influence of the surface forces on the equilibrium and stability of adsorption films. In the following description, we use the concept of disjoining pressure introduced by Derjaguin [29] to account for the fluid–solid interaction potential. This approach is equivalent to the schemes used later by Broekhoff and de Boer [31–34], and Saam and Cole [35].

For cylindrical pores, the equilibrium thickness of the adsorbed film is determined by the balance of the capillary and disjoining pressures and is given by [31,32]:

$$\Pi(h)V_L + \frac{\gamma V_L}{R_P - h} = RT\ln(P_0/P) \tag{4}$$

In the DBdB approach, the disjoining pressure $\Pi(h)$ and surface tension are considered to be independent of the pore wall curvature. Thus, the disjoining pressure of the adsorption film on the flat surface is used in Eq. (4). The disjoining pressure accounts for the sum of fluid–solid intermolecular interactions. In the case of dominant dispersion interactions, the attractive potential of the semi-infinite solid is reciprocal to the film thickness cubed ($\Pi(h) \propto h^{-3}$). In practice, however, the thickness of the adsorbed film is better described by the power law ($\Pi(h) \propto h^{-m}$), known as the Frenkel–Halsey–Hill (FHH) equation [1]. For the adsorption of nitrogen at 77.4 K on various substrates, the exponent $m \approx 2.2$–2.8 [1]. In particular, Dubinin et al. [40–43] recommended the standard N_2 isotherm, $F(h)$, on non-porous oxides at 77.4 K in the FHH form given by:

$$\ln(P_0/P) = \frac{V_L\Pi(h)}{RT} = \frac{F(h)}{RT} = \frac{K}{h^m} \tag{5}$$

with $K = 44.54$ and $m = 2.241$, where h is in Å. The FHH equation (5) is merely a two-parameter approximation of the three-parameter Harkins–Jura isotherm, $F(h)$, used by Broekhoff and de Boer [31–34].

In the DBdB method it is assumed that, as the vapor pressure increases, the condensation occurs when the limit of stability of the adsorbed films is achieved. The adsorption film is stable provided $(\partial\Pi(h)/\partial h) < 0$. The limit of stability corresponds to the critical film thickness $h = h_{cr}$, given by the algebraic equation

$$-\left(\frac{d\Pi(h)}{dh}\right)_{h=h_{cr}} = \frac{\gamma}{(R_P - h_{cr})^2} \tag{6}$$

Thus, the conditions of capillary condensation in a cylindrical pore are determined by the system of two equations (4) and (6).

Desorption from the cylindrical capillary is determined by the condition of formation of the equilibrium meniscus given by the augmented Kelvin equation, known as the Derjaguin equation [32]:

$$RT\ln(P_0/P) = \frac{2\gamma V_L + \frac{2V_L}{(R_P - h_e)}\int_{h_e}^{R_P}(R_P - h)\Pi(h)\,dh}{R_P - h_e} \tag{7}$$

Here, h_e is the thickness of the adsorbed film in equilibrium with the meniscus, given by Eq. (4). Thus, the conditions of desorption are determined by the system of two equations (4) and (7).

The DBdB method in its original [31–34] or equivalent [40] formulations was applied to many mesoporous mineral and carbonatious materials, however, it did not receive as widespread acceptance as the BJH method, which was implemented as the standard procedure in all automated commercial adsorption instruments. Recently, a variant

of the DBdB method under the nickname "BdB–FHH" (with the FHH exponent $m = 3$ in Eq. (5)) was applied to calculations of pore size distributions in MMS with cylindrical and spherical pores [27].

There were many attempts to modify the DBdB theory in order to take into account the effects of the pore wall curvature, which are expected to be appreciable in sufficiently narrow pores. Some authors introduced corrections for the liquid–vapor surface tension based on the Tolman equation considering the disjoining pressure curvature independent [44]. Others calculated the fluid–solid potential accounting for the substrate curvature, but kept the surface tension and liquid density in the adsorbed film equal to those for the bulk system [45]. After the works of Kadlec and Dubinin [46] and Burgess and Everett [47], it is well-understood that capillary condensed fluid and adsorbed films in nanopores experience effective tensile pressure (hundreds of atmospheres in the nanometer size pores) which fosters the development of instabilities in the liquid-like matter. Although the above mentioned effects have recently attracted a lot of attention [24–26], a systematic approach to this complex problem has yet to be developed (see e.g. Ref. [48]).

3. Non-local density functional theory of nitrogen and argon adsorption in MMS

The DFT of inhomogeneous fluids [49] bridges the gap between the molecular level and macroscopic approaches. There were several attempts in the literature to derive macroscopic equations of capillarity starting from the microscopic equations of DFT [3,50–52]. For example, the authors employed the DFT in the sharp-kink (slab) approximation [3,51] assuming that the properties of an adsorbed film are similar to those of a bulk liquid. Below, we use the NLDFT without any additional assumptions. The NLDFT model employed here correctly describes the local fluid structure near curved solid walls and quantitatively agrees with the molecular simulations [15]. Therefore, the NLDFT approach may serve as a benchmark for macroscopic methods such as the DBdB method.

3.1. Theory

In the DFT approach [49], adsorption isotherms in model pores are calculated based on the intermolecular potentials of the fluid–fluid and solid–fluid interactions. To describe the capillary condensation/desorption of nitrogen and argon in the pores of MMS, we employed the NLDFT model of Lennard-Jones (LJ) fluids in the Tarazona's smoothed density approximation [53]. The local density $\rho(\mathbf{r})$ of the adsorbate confined in a pore at a given chemical potential μ and temperature T is determined by minimization of the grand thermodynamic potential Ω, given as the functional:

$$\Omega[\rho(\mathbf{r})] = F_{\mathrm{HS}}[\rho(\mathbf{r})] + \frac{1}{2} \times \int\int \mathrm{d}\mathbf{r}\,\mathrm{d}\mathbf{r}'\rho(\mathbf{r})\rho(\mathbf{r}')\Phi_{\mathrm{attr}}(|\mathbf{r}-\mathbf{r}'|) - \int \mathrm{d}\mathbf{r}\,\rho(\mathbf{r})[\mu - U_{\mathrm{ext}}(\mathbf{r})] \quad (8)$$

The first term on the right hand side, $F_{\mathrm{HS}}[\rho(\mathbf{r})]$, is the non-local free energy functional of hard spheres. The second term is the mean-field free energy due to attractive interactions, $\Phi_{\mathrm{attr}}(r)$, which were calculated according to the Weeks–Chandler–Andersen scheme [54], and $U_{\mathrm{ext}}(\mathbf{r})$is the potential imposed by the pore walls. We assume that $U_{\mathrm{ext}}(\mathbf{r})$ refers mostly to the interactions of fluid molecules with the external cylindrical layer of oxygen atoms of the pore wall [55].

For the density distribution $\rho(r)$ the excess adsorption per unit area of cylindrical pore is calculated as:

$$N_{\mathrm{S}}(P/P_0) = \frac{2}{D_{\mathrm{in}}}\int_0^{D/2}\rho(r)r\,\mathrm{d}r - \frac{D_{\mathrm{in}}}{4}\rho_{\mathrm{g}}(P/P_0) \quad (9)$$

Here, $\rho_{\mathrm{g}}(P/P_0)$ is the bulk gas density at a given relative pressure, P/P_0; $D_{\mathrm{in}} = D - \sigma_{\mathrm{ss}}$ is the "internal" pore diameter, which is the diameter between the centers of oxygen atoms in the external layer of the pore wall, D, less the effective diameter of oxygen, $\sigma_{\mathrm{ss}} = 2.76$ Å. For low-temperature nitrogen and argon isotherms, the distinction between absolute and excess adsorption becomes appreciable in large pores.

Table 1
Parameters of the intermolecular interactions in the NLDFT model [10,19,20]

Adsorbate	Fluid–fluid			Solid–fluid	
	ε_{ff}/k_B (K)	σ_{ff} (Å)	d_{HS} (Å)	$\rho_S\varepsilon_{sf}/k_B$ (K/Å^2)	σ_{sf} (Å)
N_2	94.45	3.575	3.575	22.53	3.17
Ar	118.05	3.305	3.380	26.20	3.00

ε_{ff}/k_B and σ_{ff} are, respectively, the well depth and the distance parameter of the LJ potential. Fluid–fluid interactions are truncated at $5\sigma_{ff}$. d_{HS} is the diameter of hard spheres. $\rho_S\varepsilon_{sf}/k_B$ and σ_{sf} are, respectively, the energetic and distance parameters of the fluid–wall interactions.

3.2. Parameters of intermolecular potentials

The parameters of fluid–fluid interactions (Table 1) were chosen to reproduce the bulk properties of nitrogen and argon at low temperatures, including liquid–gas coexistence densities, saturation pressure, and surface tension of free liquid–gas interface [20]. The parameters of solid–fluid interactions were obtained by fitting the calculated adsorption isotherms on an open surface to the standard nitrogen and argon isotherms on non-porous oxides [40]. The intermolecular parameters used in this work have been described in our previous publications [10,19–21,23].

3.3. Capillary condensation and hysteresis in cylindrical pores of MMS

A typical example of a capillary condensation isotherm calculated by means of the NLDFT model is presented in Fig. 1. The data represent argon sorption at 87.3 K in 4.8 nm cylindrical siliceous pore. The adsorption and desorption isotherms form a wide hysteresis loop. The NLDFT model predicts that in the region of hysteresis, there are two solutions for equilibrium states which correspond to the local minima of the grand potential at a given chemical potential. The plot of the grand potential corresponding to the states on the adsorption and desorption isotherms is given at the bottom. The *equilibrium transition* corresponds to the conditions at which the two states have equal grand potentials. In the hysteresis region, the solution with a smaller grand potential

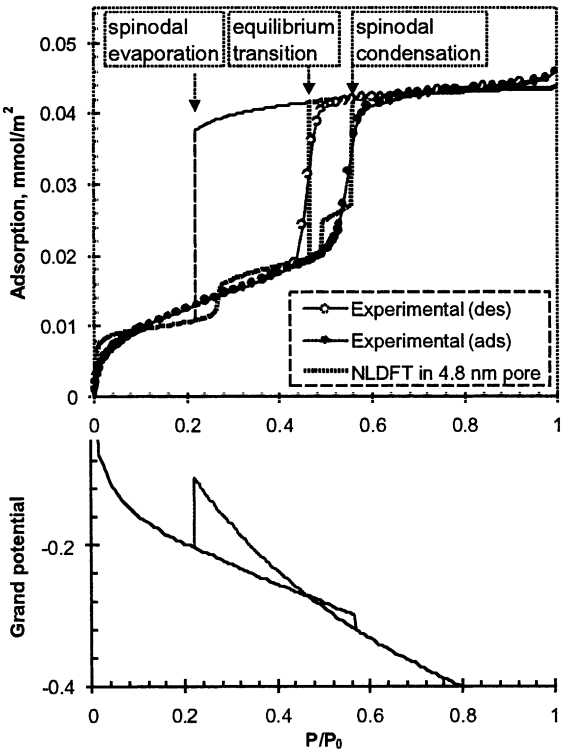

Fig. 1. Comparison of the NLDFT isotherm of Ar at 87.3 K in a 4.8 nm cylindrical pore with the corresponding isotherm on enlarged MCM-41 type material (sample designated (5.1) in Ref. [39]). The arrows indicate (from right to left) the relative pressures of spinodal condensation, equilibrium transition, and spinodal evaporation calculated by NLDFT.

corresponds to the stable branch of the isotherm, while the other corresponds to the metastable branch. Above the equilibrium transition pressure, the vapor-like states on the adsorption branch are metastable with respect to the equilibrium liquid-like configurations on the desorption branch. The metastable adsorption branch terminates at a vapor-like spinodal, where the limit of stability of the metastable states is achieved and the fluid spontaneously condenses into a liquid-like state. This determines the condensation step on the adsorption isotherm. Below the equilibrium transition pressure, the desorption branch is metastable with respect to the stable adsorption branch. The desorption branch terminates at a liquid-like spinodal, which corresponds to the spontaneous evaporation.

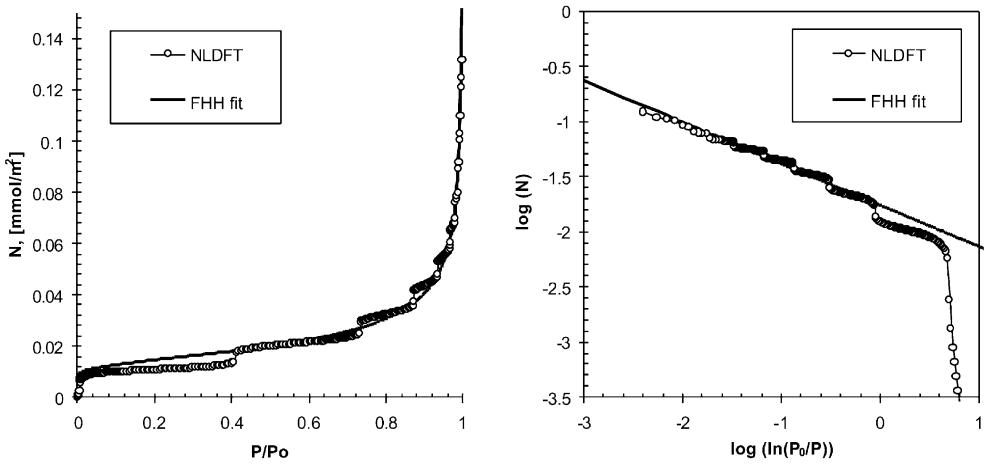

Fig. 2. The NLDFT excess isotherm of Ar at 87.3 K in a 89 nm cylindrical pore ($270\sigma_{ff}$), and its fit with the FHH equation: (a) in pressure coordinates, (b) in coordinates of the FHH equation.

It was shown previously, that in open-ended cylindrical pores the metastable liquid-like states cannot be observed and the evaporation/desorption should occur at the equilibrium transition pressure [56]. Thus, the theoretical desorption step corresponds to the equilibrium transition, while the condensation step corresponds to the spinodal spontaneous transition. To emphasize the unavailability of the metastable desorption states in adsorption experiments with MMS, the corresponding branch was plotted using a thin line and the remaining hysteretic isotherm using a bold one. These theoretical predictions perfectly agree with experimental data collected on a sample of enlarged MCM-41 type adsorbent [39]. The step-wise behavior of the adsorption branch prior to condensation is attributed to the obvious simplifications of the theoretical model, which implies a structureless energetically homogeneous pore wall. However, this simplification does not affect the positions of equilibrium and spontaneous transitions.

4. Comparison of NLDFT with macroscopic theories

To provide a fair comparison with the macroscopic theories, the thickness of the multilayer adsorption film was obtained by fitting the NLDFT adsorption isotherm in a large pore to the FHH equation in the range of relative pressures from ≈0.4 to 1 (Fig. 2). The parameters of the FHH equation used for N_2 at 77.4 K were the same as recommended by Dubinin et al. [40]. The parameters for Ar at 87.3 K are listed in Table 2.

The NLDFT adsorption and desorption isotherms were calculated in cylindrical pores 2–100 nm. The relative pressures of the equilibrium desorption and spinodal condensation transitions predicted by NLDFT are plotted in Fig. 3 in comparison with the predictions of the KC equations (1) and (2). As expected, in the limit of large pores, the line of equilibrium transitions asymptotically approaches the Kelvin equation for hemispherical meniscus, and the line of spontaneous capillary condensation asymptotically approaches the Kelvin equation for cylindrical meniscus. The width of the hysteresis loop can be estimated by the asymptotic equation (3). However, as the pore size decreases, the surface forces come forefront and deviations from the KC

Table 2
Parameters of the DBdB theory for nitrogen (77.4 K) and argon (87.3 K) adsorption in cylindrical pores of siliceous materials

	γ (mN/m)	V_m (cm^3/mol)	K	m
N_2 at 77.4 K	8.88	34.66	44.54	2.241
Ar at 87.3 K	12.5	28.68	73.17	2.665

γ is the liquid–gas surface tension, V_m is the molar volume of bulk liquid, K and m are parameters of the FHH isotherm on an open surface (Eq. (5)).

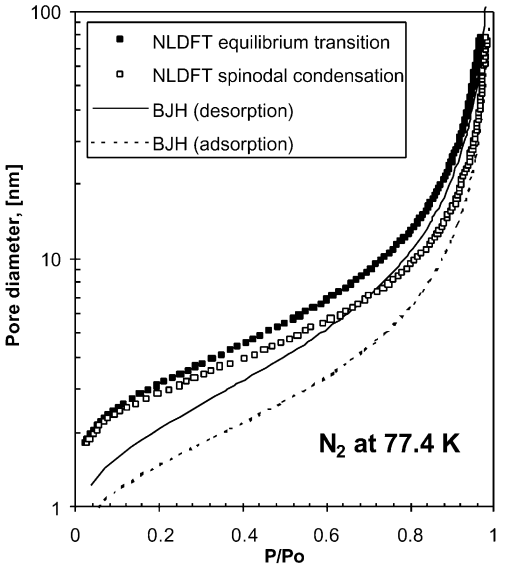

Fig. 3. Capillary hysteresis of nitrogen in cylindrical pores at 77.4 K. Equilibrium desorption (■) and spinodal condensation (□) pressures predicted by the NLDFT in comparison with the results of KC equations (BJH method) for hemispherical (—) and cylindrical (· · ·) meniscii.

equations become appreciable even for pores as large as 10–20 nm.

The comparison of the NLDFT model with the DBdB model shows that the two approaches are in agreement for pores wider than ≈7 nm (Figs. 4 and 5). For both nitrogen and argon, the equilibrium and spinodal capillary condensation transitions predicted by the NLDFT model can be approximated by the DBdB equations. However, as the pore size decreases below 7 nm, the deviations become progressively more and more substantial, especially for the position of the condensation spinodal. The DBdB theory implies wider hysteresis loops. The NLDFT model predicts the critical pore size of capillary condensation equal to ≈2 nm, which is approximately the minimum pore size in which N_2 capillary condensation at 77 K was experimentally observed [10]. At the critical pore size, the hysteresis loop vanishes, and the line of spinodal condensation merges with the line of equilibrium transitions (Figs. 4 and 5). It is worth noting that the DBdB theory fails to predict the capillary critical point at all.

5. Comparison with experiments

In Figs. 6–8, we compare experimental adsorption–desorption isotherms of N_2 at 77 K and Ar at 87 K on enlarged MCM-41-type samples [37–39] with the NLDFT isotherms in single cylindrical pores. The pore sizes were chosen from the inflection points of the experimental N_2 desorption isotherm. Both for N_2 and Ar, the

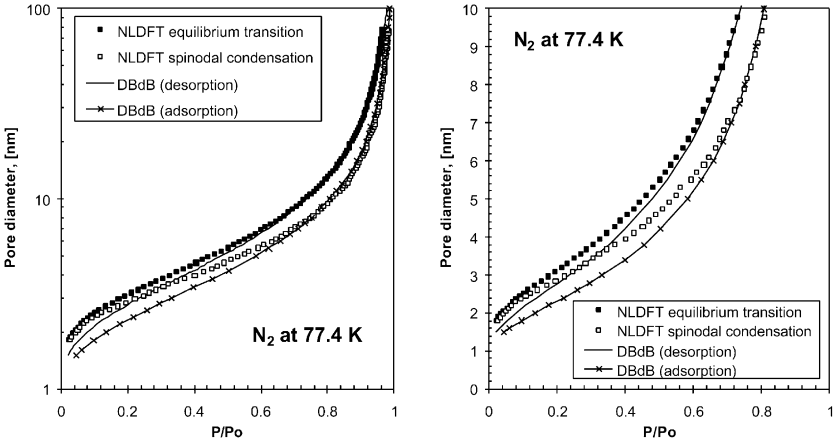

Fig. 4. Capillary hysteresis of nitrogen in cylindrical pores at 77.4 K. Equilibrium desorption (■) and spinodal condensation (□) pressures predicted by the NLDFT in comparison with the results of the DBdB theory for desorption (–) and adsorption (-•-).

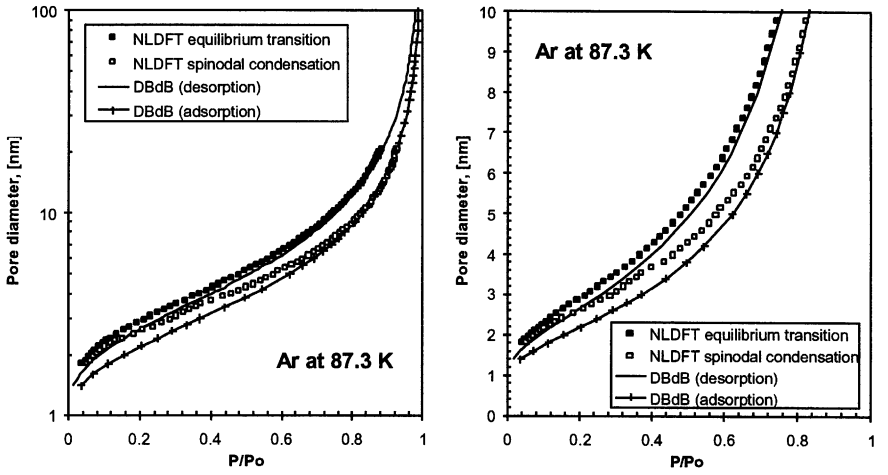

Fig. 5. Capillary hysteresis of argon in cylindrical pores at 87.3 K. Equilibrium desorption (■) and spinodal condensation (□) pressures predicted by the NLDFT in comparison with the results of the DBdB theory for desorption (—) and adsorption (-•-).

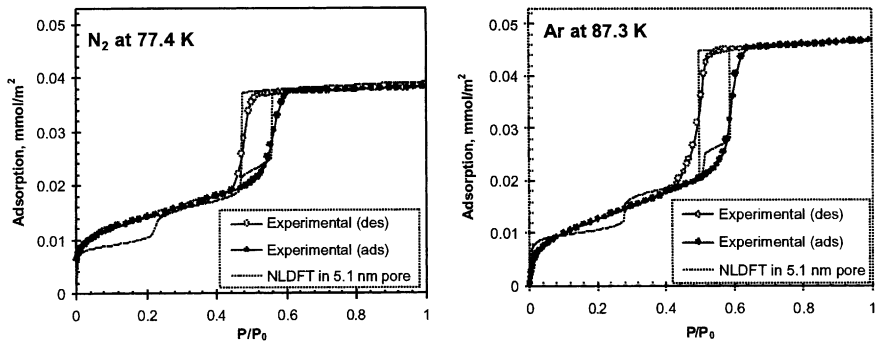

Fig. 6. Comparison of the NLDFT isotherms of N_2 at 77.4 K (left) and Ar at 87.3 K (right) in a 5.1 nm cylindrical pore with the corresponding isotherms on enlarged MCM-41 type material (sample designated (5.5) in Refs. [37–39]). The experimental N_2 and Ar isotherms are reduced by the surface areas of 770 and 730 m^2/g, respectively.

calculations reproduce almost quantitatively the main features of the experimental isotherms: (1) the thickness of the multilayer adsorption film, (2) the pressure of spontaneous capillary condensation, (3) the total amount adsorbed in a pore of a given size, and (4) the pressure of spontaneous evaporation (desorption). The stepwise behavior of theoretical isotherms in the region of the mono- and multilayer adsorption prior to condensation is caused by a structureless pore wall model, which neglects the energetic heterogeneity of the silica surface. The "vertical" condensation/evaporation transitions are not observed in experiments due to the pore size heterogeneity, and possibly, due to some degree of non-uniformity of the pore channels. However, the calculated condensation and equilibrium transitions correspond to the inflection points of the experimental adsorption and desorption isotherms, respectively. The observed agreement between the theory and experiment confirms the conclusion that capillary condensation in cylindrical pores larger that $\approx$5 nm occurs at the limit of stability of the adsorption film (vapor-like spinodal), while desorption takes place at the equilibrium pressure of liquid–vapor coexistence (Figs. 6–8).

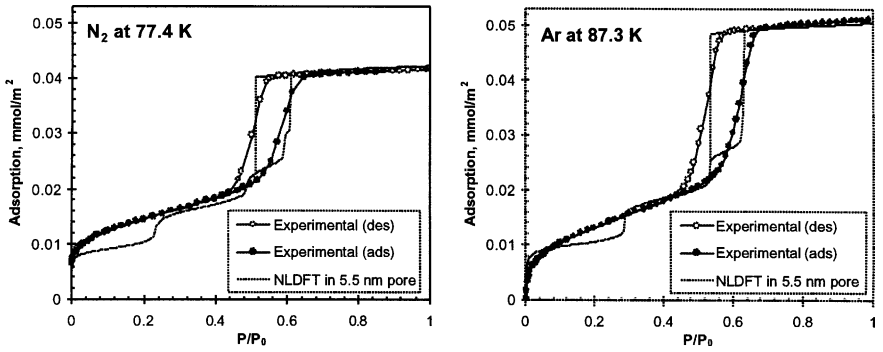

Fig. 7. Comparison of the NLDFT isotherms of N_2 at 77.4 K (left) and Ar at 87.3 K (right) in a 5.5 nm cylindrical pore with the corresponding isotherms on enlarged MCM-41 type material (sample designated (6.0) in Refs. [37–39]). The experimental N_2 and Ar isotherms are reduced by the surface areas of 760 and 740 m^2/g, respectively.

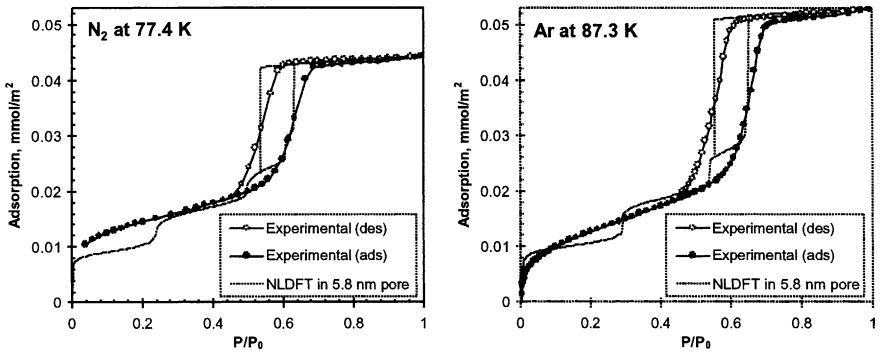

Fig. 8. Comparison of the NLDFT isotherms of N_2 at 77.4 K (left) and Ar at 87.3 K (right) in a 5.8 nm cylindrical pore with the corresponding isotherms on enlarged MCM-41 type material (sample designated (6.5) in Refs. [37–39]). The experimental N_2 and Ar isotherms are reduced by the surface area of 660 m^2/g.

Note that the reported pore dimensions for the samples presented in Figs. 6–8 exceeded our estimates by $\approx$0.3–0.7 nm. These deviations seem to be within reasonable bounds since the authors [37–39] used a geometrical relation for an ideal hexagonal array of uniform channels of circular cross-section and the wall density of amorphous silica. This approach gives plausible estimates, however, its accuracy can not be justified for real samples with pore size and other uncontrolled heterogeneities. As seen from Fig. 9, the pore size distributions in the samples analyzed are appreciably broad. Comparison of the NLDFT isotherms with the experimental data on other MCM-41 type materials [20,36], and also with the results of MC simulations is presented in our recent paper [15].

It is worth noting that the parameters of intermolecular interactions used in the NLDFT calculations presented here were determined in our earlier publications [10,19,20], when the experimental data on large-pore MCM-41 type materials were unavailable. The remarkable agreement with the experimental data shown in Figs. 6–8 demonstrates the power of the NLDFT in predicting adsorption in nanopores.

6. Calculation of pore size distributions from adsorption and desorption isotherms

To calculate the pore size distributions, the experimental isotherm is represented as a

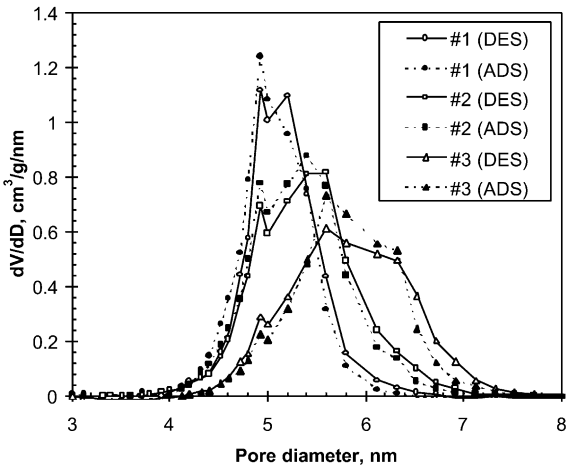

Fig. 9. The pore size distributions of enlarged MCM-41 type materials [37,38] shown in Figs. 6–8 calculated from adsorption (···) and desorption (—) branches of nitrogen isotherms by the NLDFT method [23].

combination of theoretical isotherms in individual pores:

$$N_{\exp}(P/P_0) = \int_{D_{\min}}^{D_{\max}} N_S(D_{in}, P/P_0)\varphi_S(D_{in})\,dD_{in} \tag{10}$$

where $N_S(D_{in}, P/P_0)$ is the kernel of the theoretical isotherms in pores of different diameters, $\varphi_S(D_{in})$ is the pore size distribution. Two kernels of theoretical isotherms were constructed using the NLDFT model. The first kernel consists of the equilibrium desorption isotherms, and the second of the metastable adsorption branches. These kernels were employed for calculations of pore size distributions from the experimental desorption and adsorption isotherms, respectively. The integral equation (10) was represented as a matrix equation and inverted using the discrete Tikhonov regularization method, which minimizes the 2-norm of the solution vector [57]. Details of calculations are presented elsewhere.

In Fig. 9, we show pore size distributions for the enlarged MCM-41 samples [37,38] calculated from the N_2 experimental desorption branches using the desorption kernel, and from the N_2 experimental adsorption branches using the adsorption kernel. The pore size distributions obtained from the desorption and adsorption branches practically coincide, indicating the consistency of our approach.

7. Conclusions

The NLDFT model of capillary condensation in cylindrical pores was compared with the macroscopic DBdB theory and the experimental adsorption/desorption isotherms of nitrogen and argon on enlarged MCM-41 type materials. The adsorption–desorption isotherms predicted by NLDFT are found to be in quantitative agreement with the experimental measurements. The results prove that in relatively large pores, the experimental capillary condensation occurs when the adsorption film approaches the limit of thermodynamic stability (vapor-like spinodal). For nitrogen at 77.4 K and argon at 87.3 K, the spontaneous spinodal condensation is observed in pores larger than 5–6 nm in diameter. On the desorption path, the metastable states are not achieved, and evaporation occurs at the conditions of liquid–vapor coexistence. The DBdB with consistently determined thickness of the adsorbed layer (disjoining pressure isotherm) can be justified for pores wider than ≈7 nm. As the pore size decreases, the deviations become progressively more and more substantial, and the DBdB theory predicts much wider hysteresis loops. The KC equations, which constitute the basis of the traditional BJH method for pore size distribution analysis, are in error even for pores as large as 20 nm.

The NLDFT method has been developed for calculating pore size distributions from both the adsorption and desorption isotherms. Consistent results have been obtained using the adsorption and desorption branches of the experimental isotherms on MCM-41 type materials with cylindrical pores as small as ≈5 nm. For samples with smaller cylindrical pores, we recommend to employ the desorption data (in the case of hysteresis) for the pore size distribution analysis; the use of the adsorption data is hampered by the lack of theoretical description of metastable adsorption states in pores smaller than 5 nm. The latter issue will be considered elsewhere.

Acknowledgements

This work was supported in parts by the TRI/Princeton exploratory research program, EPA grant R825959-010, and Quantachrome Corp.

References

[1] S.J. Gregg, K.S.W. Sing, Adsorption, Surface Area and Porosity, Academic Press, London, 1982.
[2] F. Rouquerol, J. Rouquerol, K.S.W. Sing, Adsorption by Powders and Porous Solids: Principles, Methodology and Applications, Academic Press, San Diego, 1999.
[3] R. Evans, U.M.B. Marconi, P. Tarazona, J. Chem. Soc. Faraday Trans. 2 (82) (1986) 1763.
[4] R. Evans, J. Phys. Condens. Matter 2 (1990) 8989.
[5] L.D. Gelb, K.E. Gubbins, R. Radhakrishnan, M. Sliwinska-Bartkowiak, Rep. Prog. Phys. 62 (1999) 1573.
[6] A.Z. Zsigmondy, Z. Anorg. Chem. 1 (1911) 356.
[7] L.H. Cohan, J. Am. Chem. Soc. 60 (1938) 433.
[8] E.P. Barrett, L.G. Joyner, P.H. Halenda, J. Am. Chem. Soc. 73 (1951) 373.
[9] P.I. Ravikovitch, S.C. Ó Domhnaill, A.V. Neimark, F. Schüth, K.K. Unger, Langmuir 11 (1995) 4765.
[10] P.I. Ravikovitch, D. Wei, W.T. Chueh, G.L. Haller, A.V. Neimark, J. Phys. Chem. B 101 (1997) 3671.
[11] D.H. Everett, in: E.A. Flood (Ed.), The Solid–Gas Interface, vol. 2, Marcel Decker, New York, 1967.
[12] M.W. Maddox, K.E. Gubbins, Int. J. Thermophys. 15 (1994) 1115.
[13] M.W. Maddox, J.P. Olivier, K.E. Gubbins, Langmuir 13 (1997) 1737.
[14] L.D. Gelb, K.E. Gubbins, Langmuir 15 (1999) 305.
[15] A.V. Neimark, P.I. Ravikovitch, A. Vishnyakov, Phys. Rev. E 62 (2000) R1493.
[16] A. de Keizer, Th. Michalski, G.H. Findenegg, Pure & Appl. Chem. 63 (1991) 1495.
[17] M. Miahara, H. Kanda, T. Yoshioka, M. Okazaki, in: F. Meunier (Ed.), Fundamentals of Adsorption 6, Elsevier, Paris, 1998, p. 249.
[18] C. Lastoskie, N. Quirke, K.E. Gubbins, Stud. Surf. Sci. Catal. 104 (1997) 745.
[19] P.I. Ravikovitch, G.L. Haller, A.V. Neimark, Adv. Colloid Interf. Sci. 77 (1998) 203.
[20] A.V. Neimark, P.I. Ravikovitch, M. Grün, F. Schüth, K.K. Unger, J. Colloid Interf. Sci. 207 (1998) 159.
[21] P.I. Ravikovitch, G.L. Haller, A.V. Neimark, Stud. Surf. Sci. Catal. 117 (1998) 77.
[22] A.V. Neimark, P.I. Ravikovitch, Stud. Surf. Sci. Catal. 128 (2000) 51.
[23] P.I. Ravikovitch, A.V. Neimark, Stud. Surf. Sci. Catal. 129 (2000) 597.
[24] C.G. Sonwane, S.K. Bhatia, Chem. Eng. Sci. 53 (1998) 3143.
[25] S. Inoue, S.Y. Hanzawa, K. Kaneko, Langmuir 14 (1998) 3078.
[26] H.Y. Zhu, L.A. Ni, G.Q. Lu, Langmuir 15 (1999) 3632.
[27] W.W. Lukens Jr., P. Schmidt-Winkel, D. Zhao, J. Feng, G.D. Stucky, Langmuir 15 (1999) 5403.
[28] N.V. Churaev, G. Starke, J. Adolphs, J. Colloid Interf. Sci. 221 (2000) 246.
[29] B.V. Derjaguin, Acta Physicochim. URSS 12 (1940) 181.
[30] B.V. Derjaguin, N.V. Churaev, J. Colloid Interf. Sci. 54 (1976) 157.
[31] J.C.P. Broekhoff, J.H. de Boer, J. Catal. 9 (1967) 8.
[32] J.C.P. Broekhoff, J.H. de Boer, J. Catal. 9 (1967) 15.
[33] J.C.P. Broekhoff, J.H. de Boer, J. Catal. 10 (1968) 368.
[34] J.C.P. Broekhoff, J.H. de Boer, J. Catal. 10 (1968) 377.
[35] W.F. Saam, M.W. Cole, Phys. Rev. B 11 (1975) 1086.
[36] Q. Huo, D.I. Margolese, G.D. Stucky, Chem. Mater. 8 (1996) 1147.
[37] A. Sayari, P. Liu, M. Kruk, M. Jaroniec, Chem. Mater. 9 (1997) 2499.
[38] M. Kruk, M. Jaroniec, A. Sayari, Langmuir 13 (1997) 6267.
[39] M. Kruk, M. Jaroniec, Chem. Mater. 12 (2000) 222.
[40] M.M. Dubinin, L.I. Kataeva, V.I. Ulin, Bull. Acad. Sci. USSR Chem. 26 (1977) 459.
[41] M.M. Dubinin, L.I. Kataeva, Bull. Acad. Sci. USSR Chem. 26 (1977) 464.
[42] M.M. Dubinin, L.I. Kataeva, Bull. Acad. Sci. USSR Chem. 29 (1980) 159.
[43] M.M. Dubinin, L.I. Kataeva, Bull. Acad. Sci. USSR Chem. 29 (1980) 321.
[44] M.M. Dubinin, L.I. Kataeva, V.I. Ulin, Bull. Acad. Sci. USSR Chem. 30 (1981) 25.
[45] C. Bauer, S. Dietrich, Preprint, WUB 00-04, Bergische Universitat Wuppertal, 2000.
[46] O. Kadlec, M.M. Dubinin, J. Colloid Interf. Sci. 31 (1969) 479.
[47] C.G.V. Burgess, D.H. Everett, J.Colloid Interf. Sci. 33 (1970) 611.
[48] R. Tsekov, K.W. Stöckelhuber, B.V. Toshev, Langmuir 16 (2000) 3502.
[49] R. Evans, in: D. Henderson (Ed.), Fundamentals of Inhomogeneous Fluids, Marcel Dekker, New York, 1992 (Chapter 5).
[50] H.T. Davis, Statistical Mechanics of Phases, Interfaces, and Thin Films, Wiley-VCH, New York, 1996 (Chapter 13).
[51] T. Bieker, S. Dietrich, Physica A 252 (1998) 85.
[52] R.H. Nilson, S.K. Griffiths, J. Chem. Phys. 111 (1999) 4281.
[53] P. Tarazona, U.M.B. Marconi, R. Evans, Mol. Phys. 60 (1987) 573.
[54] J.D. Weeks, D. Chandler, H.C. Andersen, J. Chem. Phys. 54 (1971) 5237.
[55] G.J. Tjatjopoulos, D.L. Feke, J.A. Mann Jr., J. Phys. Chem. 92 (1988) 4006.
[56] A. Papadopoulou, F. van Swol, U.M.B. Marconi, J. Chem. Phys. 97 (1992) 6942.
[57] C.L. Lawson, R.J. Hanson, Solving Least Squares Problems, SIAM, Philadelphia, 1995.